NACA

RESEARCH MEMORANDUM

THE ROLLING EFFECTIVENESS OF WING-TIP AILERONS AS

DETERMINED BY ROCKET-POWERED TEST VEHICLES

AND LINEAR SUPERSONIC THEORY

By Carl A. Sandahl, H. Kurt Strass,
and Robert O. Piland

Langley Aeronautical Laboratory
Langley Air Force Base, Va.

FOR REFERENCE

NOT TO BE TAKEN FROM THIS ROOM

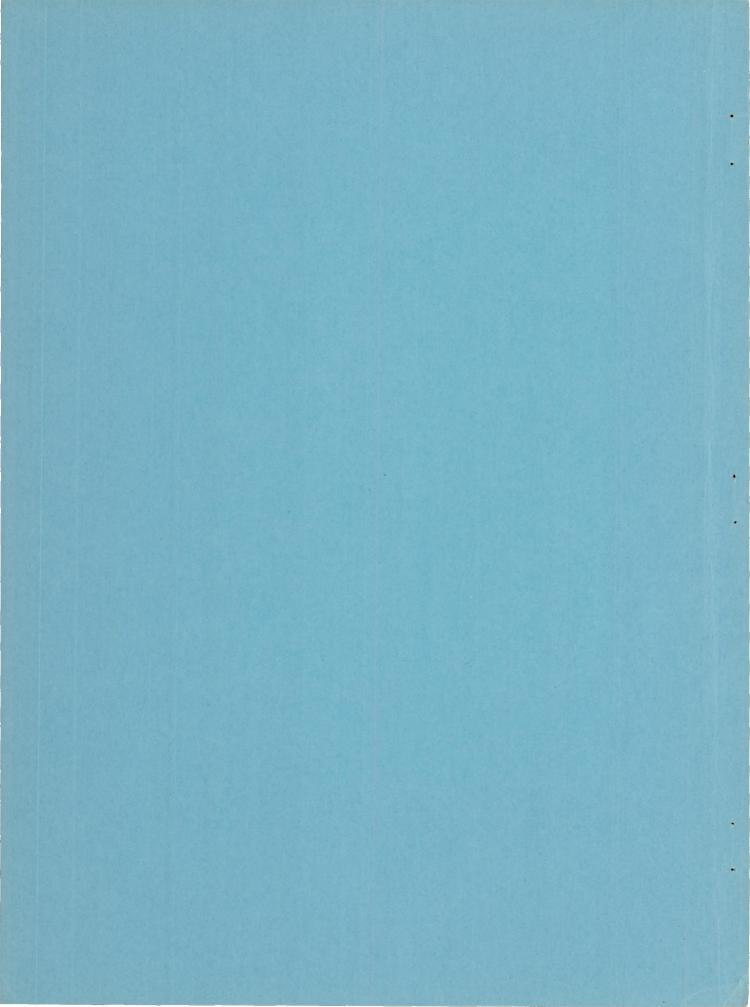CLASSIFICATION CHANGED TO UNCLASSIFIED

AUTHORITY: NACA RESEARCH ABSTRACT NO. 109

DATE: NOVEMBER 14, 1956   WHT

NATIONAL ADVISORY COMMITTEE
FOR AERONAUTICS
WASHINGTON
August 29, 1950

NATIONAL ADVISORY COMMITTEE FOR AERONAUTICS

———

RESEARCH MEMORANDUM

———

THE ROLLING EFFECTIVENESS OF WING-TIP AILERONS AS

DETERMINED BY ROCKET-POWERED TEST VEHICLES

AND LINEAR SUPERSONIC THEORY

By Carl A. Sandahl, H. Kurt Strass,
and Robert O. Piland

SUMMARY

The rolling effectiveness and drag of half-delta wing-tip ailerons on rectangular and tapered wings sweptback 0° and 45° have been determined by means of rocket-powered test vehicles over the Mach number range from about 0.6 to 1.7. The rolling effectiveness of the wing-tip ailerons was found to be relatively uniform over the test Mach number range and was lower at subsonic speeds and higher at supersonic speeds than that of plain partial-span ailerons of equal area. Increasing the wing sweepback from 0° to 45° and decreasing the wing taper ratio from 1.0 to 0.45 decreased the rolling effectiveness. Values of rolling effectiveness calculated by means of linear supersonic theory agreed well with the experimental results. With unswept wings, the wing-tip ailerons had no measurable effect on the wing drag coefficient. For the sweptback wing configuration the wing-tip ailerons caused the transonic drag rise to occur at a lower Mach number.

INTRODUCTION

Lateral controls consisting of small deflectable lifting surfaces attached to the tips of the wings of pilotless and piloted aircraft have received some consideration. Some of the advantages claimed for such wing-tip lateral controls are: large rolling-moment arm available; possibility of locating the hinge axis to reduce hinge moments; and the possibility of installing full-span high-lift devices on the main wings. Probably the main disadvantage of such controls is the structural problem entailed in the design of practical configurations.

Previous work with wing-tip ailerons on delta-plan-form wings at high-subsonic, transonic, and supersonic speeds (reference 1) has shown

that such ailerons have favorable rolling-effectiveness characteristics in comparison with trailing-edge controls. As a continuation of this work, half-delta tip ailerons have been investigated on several rectangular and tapered wings having 0° and 45° sweepback. The rolling effectiveness was determined by means of rocket-propelled test vehicles with the use of the technique described in reference 2 by means of which the variation of wing-aileron rolling effectiveness with Mach number can be obtained. In addition to the rolling power measurements the variation of total drag coefficient with Mach number was obtained. It is the purpose of this paper to present these experimental results and to compare them with results for plain partial-span ailerons of equal area. The rolling-effectiveness results are also compared with those obtained by means of linear supersonic theory.

SYMBOLS

$pb/2V$ wing-tip helix angle, radians

p rolling velocity, radians

b total wing span, feet

V flight velocity, feet per second

C_D total drag coefficient based on total exposed area of wing and aileron (1.720 sq ft for present tests)

C_{D_w} wing drag coefficient based on total exposed area of wing and aileron

M Mach number

R Reynolds number

A aspect ratio based on total wing span and total area of two wings obtained by extending leading and trailing edges to model center line

$\Lambda_{c/2}$ sweepback of 50-percent-chord line of wing, degrees

λ_w taper ratio of wing excluding aileron

S total exposed wing area including ailerons (1.720 sq ft)

S_a total aileron area (0.156 sq ft for three-panel model)

$S_o = S - S_a$ (1.563 sq ft for three-panel model)

c   local wing chord parallel to model center line

δ   deflection of each aileron obtained by averaging the deflections
                of the three ailerons, degrees

i   incidence of each wing panel obtained by averaging the incidence
                values of the three wing panels, degrees

TEST VEHICLES AND TESTS

The general arrangement of the test vehicles is shown in figures 1
and 2. The geometric details of the wing-aileron configurations tested
are shown in figure 3.

All of the wings, exclusive of the ailerons, had NACA 65A009 airfoil
sections in planes parallel to the model center line, total exposed wing
areas of 1.720 square feet, and semispans of 1.357 feet. The resulting
aspect ratios are listed in table I. The total aileron area was held
constant at 10 percent of the basic exposed wing area which corresponds
to 9.1 percent of the total exposed area of the wing and aileron. The
control deflection and the wing incidence were set at the desired values
of 5° and 0°, respectively, during construction and were nonadjustable.
The actual measured values of aileron deflection and wing incidence are
listed in table I. The theoretical hinge line passed through a point
located at two-thirds of the aileron root chord behind the wing leading
edge.

The test vehicles were accelerated by a two-stage rocket-propulsion
system to a Mach number of about 1.7. During coasting flight following
burnout of the rocket motor, time histories of the rolling velocity pro-
duced by the ailerons (obtained with modified spinsonde equipment (refer-
ence 3)) and the flight-path velocity (obtained with Doppler radar) were
recorded. These data, in conjunction with atmospheric measurements
obtained with radiosondes, permitted the evaluation of the rolling-

effectiveness parameter $\frac{pb}{2V}\Big/\delta$ as a function of Mach number. The drag

coefficient of the test vehicles was obtained by arithmetic differentia-
tion of the flight-path velocity-time history. The scale of the tests
is indicated by the curve of Reynolds number against Mach number shown
in figure 4. A more complete description of the test method is given in
reference 2.

ACCURACY AND CORRECTIONS

The error in the determination of the quantity $\frac{pb}{2V}\Big/\delta$ for any one model is estimated to be within ±0.0004 and ±0.0002 at the lowest and highest test Mach numbers, respectively. However, experience has shown that the $\frac{pb}{2V}\Big/\delta$ obtained from nominally identical models may vary (because of small physical differences in the models) by as much as ±0.0007 and ±0.0003 at the lowest and highest test Mach numbers, respectively.

The errors in the drag coefficient and the Mach number are estimated to be within ±0.002 and ±0.005, respectively.

The values of $\frac{pb}{2V}\Big/\delta$ obtained during flight deviated slightly from steady-state values because the models experienced a continuous rolling acceleration or deceleration. The deviation is small, however, being a maximum of about 10 percent in the Mach number range from $M = 0.85$ to $M = 1.0$ for those models for which an abrupt change in rolling effectiveness was obtained. The deviation was negligible over the remainder of the Mach number range investigated.

The $\frac{pb}{2V}\Big/\delta$ values have been corrected to zero wing incidence. The correction, which was determined experimentally by means of test vehicles similar to those of the present tests except that the ailerons were undeflected and the wings were set at angles of incidence, is given by the following relations:

For untapered wings

$$\frac{\Delta pb}{2V} = \frac{1.5i}{57.3}$$

and for tapered wings

$$\frac{\Delta pb}{2V} = \frac{1.6i}{57.3}$$

RESULTS AND DISCUSSION

The variation of the rolling-effectiveness parameter $\frac{pb}{2V}\bigg/\delta$ with Mach number for the configurations tested is shown in figure 5. All of the configurations tested exhibited a relatively uniform rolling effectiveness over the Mach number range investigated with the exception of the configuration having the reverse half-delta aileron (model 5) for which an abrupt change in effectiveness was obtained in the Mach number range from 0.85 to 0.95. This same configuration (model 5) had the highest effectiveness of those tested. Increasing the wing sweepback from 0° to 45° is shown by the results for configurations 1 and 2 ($\lambda_W = 1.0$) and 3 and 4 ($\lambda_W = 0.45$) to decrease the rolling effectiveness, particularly at the subsonic and highest supersonic speeds investigated. Increasing the taper ratio from 0.45 to 1.0 increased the rolling effectiveness probably because the untapered wing tested has a larger area in the zone of influence of the tip aileron which would produce a larger rolling moment.

A comparison of the rolling effectiveness of half-delta wing-tip ailerons with that of plain partial-span ailerons of equal area obtained from reference 4 is shown in figure 6. Both the plain aileron and the tip-aileron configurations had the same basic wing plan forms. For both sweepback angles, the half-delta tip ailerons show higher effectiveness at supersonic speeds and a more nearly uniform effectiveness over the Mach number range investigated than the plain ailerons. At subsonic speeds, the rolling effectiveness, per unit aileron deflection, of the half-delta wing-tip ailerons is considerably less than that of the plain ailerons. It should be noted that, at the supersonic speeds investigated, increasing the wing sweepback from 0° to 45° reduced the effectiveness of the plain aileron considerably but had a negligible effect on the rolling effectiveness of the tip ailerons.

The variation of the rolling effectiveness with Mach number, calculated as described in the appendix with the use of methods of linear supersonic theory, is compared with experimental results in figure 7. For the two configurations considered the agreement is good.

The variation of total drag coefficient with Mach number for the configurations tested is shown in figure 8. The drag coefficient of configuration 2 was not obtained at the higher supersonic speeds because of radar-tracking difficulties. The usual beneficial effects of wing sweep are apparent. The drag of the configuration having the reverse half-delta aileron (model 5), which had a blunt round leading edge, was slightly higher than that of the comparable configuration having the apex-first half-delta aileron (model 3).

In figure 9 are plotted drag coefficients based on total exposed wing area including ailerons of identical wings with and without half-delta wing-tip ailerons. The wing drag coefficients shown in figure 9 were obtained by subtracting a fuselage drag coefficient from the total measured drag coefficient. The fuselage drag coefficient was obtained from unpublished flight tests of a wingless, finless fuselage identical to that employed in the present tests. The wing drag coefficients obtained in this way include interference effects of unknown magnitude which tend to invalidate the absolute values of wing drag coefficient obtained. However, the increments in wing drag coefficients due to the half-delta wing-tip ailerons are believed to be reliable. The results for the plain wing are unpublished and were obtained from flight tests of configurations identical to configurations 1 and 2 of the present tests except that they had no ailerons and had values of wing incidence ranging from $0°$ to $0.5°$. The drag coefficients of these plain-wing configurations having several values of wing incidence and rates of roll agreed within experimental accuracy. The drag coefficients shown in figure 9 for these configurations were those measured at approximately the $pb/2V$ values obtained by the half-delta wing-tip aileron configurations. The increments in C_{D_w} shown in figure 9 are therefore caused only by the drag and interference of the half-delta tip ailerons.

The results shown in figure 9 indicate that for $\Lambda_{c/2} = 0°$, the tip aileron had no measurable effect on the wing drag coefficient. With $\Lambda_{c/2} = 45°$, the wing-tip ailerons caused the transonic drag rise to occur at a lower Mach number.

CONCLUSIONS

The following conclusions regarding the rolling effectiveness and drag of half-delta wing-tip ailerons in the Mach number range from about 0.6 to 1.7 are based on the results of the tests reported herein:

1. The rolling effectiveness of the half-delta wing-tip ailerons was relatively uniform over the Mach number range investigated.

2. Increasing wing sweepback from $0°$ to $45°$ decreased the rolling effectiveness somewhat at the subsonic and the highest supersonic Mach numbers investigated.

3. Increasing the wing taper ratio from 0.45 to 1.0 increased the rolling effectiveness.

4. The rolling effectiveness of the wing-tip ailerons was lower than that of comparable plain ailerons at subsonic speeds but considerably higher at supersonic speeds.

5. Good agreement was obtained between the rolling effectiveness predicted by linear supersonic theory and that obtained experimentally.

6. For the unswept configuration the wing-tip ailerons had no measurable effect on the wing drag coefficient.

7. For the sweptback wing configuration, the wing-tip ailerons caused the transonic drag rise to occur at a lower Mach number.

Langley Aeronautical Laboratory
    National Advisory Committee for Aeronautics
        Langley Air Force Base, Va.

APPENDIX

DETERMINATION OF THE THEORETICAL ROLLING

EFFECTIVENESS OF WING-TIP AILERONS

By Robert O. Piland

INTRODUCTION

The rolling-effectiveness parameter $\frac{pb}{2V}\Big/\delta$ was calculated for wing-tip ailerons on a rectangular and an unswept tapered wing by means of linear theory. The equations for the rolling moments involved integrals, which due to their complexity, necessitated numerical integrations in some cases. These expressions, however, are presented in a form which will allow the calculation of $\frac{pb}{2V}\Big/\delta$ for wings of these plan forms regardless of sweep angle, aspect ratio, and Mach number, within the limits of the theory. These limits restrict the Mach number range to cases where the Mach line from the leading-edge tip lies ahead of the leading edge of the aileron ($\beta m < 1$), and the Mach line from the apex of the wing intersects the trailing edge inboard of the aileron $\left(\beta > \frac{c_r + c_t}{2h}\right)$.

SYMBOLS

The following symbols are defined in addition to those given in the section entitled "SYMBOLS" of the main body of the present paper. In some cases, symbols are redefined because their usage in the appendix is different from that in the main body of the paper.

C_{l_p} damping-in-roll coefficient $\left(\partial C_l \Big/ \partial \frac{pb}{2V}\right)_{\frac{pb}{2V} \to 0}$

C_{l_δ} rolling-moment effectiveness coefficient for two
            ailerons $\left(\partial C_l \big/ \partial \delta\right)_{\delta \to 0}$

$C_l = \frac{l}{qSb}$
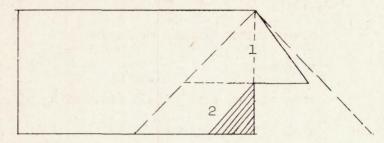
l rolling moment, positive when tending to depress right wing

q free-stream dynamic pressure

b wing span

S area of two wing panels (including ailerons)

S_a area of two ailerons

$S_o = S - S_a$

c_t chord of wing at juncture of wing and aileron

c_a chord of aileron at juncture of wing and aileron

c_r root chord of wing

h distance from center line to wing-aileron juncture

x, y coordinate axes (see fig. 10)

θ sweep of leading edge of aileron (see fig. 10)

$m = \cot \theta$

Λ sweep of leading edge of wing (see fig. 10)

$k = \tan \Lambda$

μ half the angle between the Mach lines emanating from the tip apex

$\beta = \cot \mu = \sqrt{M^2 - 1}$

φ velocity potential due to rolling

C_p pressure coefficient

RECTANGULAR WING

From a consideration of the moments acting on a wing in a steady roll the value of $\frac{pb}{2V}\big/\delta$ is given by the ratio $C_{l_\delta}\big/C_{l_p}$. Consequently, the problem is the determination of these parameters.

Rolling-Moment Effectiveness Coefficient $C_{l\delta}$

The total $C_{l\delta}$ for the configuration in the preceding sketch was determined by obtaining the respective rolling-moment contributions of regions 1 $\left(C_{l\delta_1}\right)$ and 2 $\left(C_{l\delta_2}\right)$. The pressure within the Mach cone on the wing is given in reference 5 by equation (7)(p. 33) as

$$C_p = \frac{4\delta}{\pi\beta} \frac{\beta m}{(1 + \beta m)} \sqrt{\frac{x + \beta y}{\beta m x - \beta y}}$$

The notation has been changed to comply with that of the present paper. The quantities $C_{l\delta_1}$ and $C_{l\delta_2}$, representing the rolling-moment contributions of regions 1 and 2, respectively, are obtained by integrating the pressure over the areas. In the shaded area of region 2 the pressure used is not correct since the aileron does not extend to the trailing edge of the wing. The error introduced by this approximation is believed to be small and will be discussed more fully in the following section. The rolling-moment contributions of the two areas are as follows:

$$C_{l\delta_1} = \frac{4\sqrt{\beta m}}{\beta} \frac{S_a}{Sb} \left[h + \frac{c_a}{6\beta} (3\beta m - 1) \right] \tag{1}$$
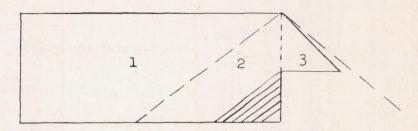
$$C_{l\delta_2} = \frac{16(\beta m)^{3/2}}{\pi\beta^2 Sb(\beta m + 1)} \left\{ \frac{(\beta m + 1)}{4} \left[h\left(c_t^2 - c_a^2\right) + \right. \right.$$

$$\left. \frac{(3\beta m - 1)\left(c_t^3 - c_a^3\right)}{6\beta} \right] \cos^{-1}\left(\frac{\beta m - 1}{\beta m + 1}\right) - \left[\frac{h\left(c_t^2 - c_a^2\right)}{2} + \right.$$

$$\left. \left. \frac{(3\beta m + 1)\left(c_t^3 - c_a^3\right)}{12\beta} \right] \sqrt{\beta m} \right\} \tag{2}$$

$$C_{l_{\delta_{Total}}} = C_{l_{\delta_1}} + C_{l_{\delta_2}} \tag{3}$$

Damping-in-Roll Coefficient C_{l_p}

The total C_{l_p} was obtained by combining the respective rolling-moment contributions of the three regions of the wing denoted in the preceding sketch. The velocity potential φ in region 1 on the wing is given on page 25 of reference 6 as $\varphi_1 = \dfrac{4py}{\beta V}$.

$$C_{l_p} = \frac{16}{\pi S b^2} \int_{y_1}^{y_2} \int_{x_1}^{x_2} (y + h) \frac{\partial \varphi}{\partial x} \, dx \, dy \tag{4}$$

By performing the operations upon φ, indicated in equation (4), $C_{l_{p1}}$ is obtained

$$C_{l_{p1}} = 2 \frac{A c_t}{\beta b} \left[\frac{1}{3} - \frac{c}{\beta b}(2\beta m + 1) + \frac{4c^2}{3\beta^2 b^2}(3\beta^2 m^2 + 3\beta m + 1) - \right.$$

$$\left. \frac{2c^3}{3b^3\beta^3}(4\beta^3 m^3 + 6\beta^2 m^2 + 4\beta m + 1) \right] \tag{5}$$

The potential $\varphi_{2,3}$ in regions 2 and 3 on the wing was determined from the method of Evvard (reference 7).

$$\varphi_{2,3} = \frac{p}{\pi} \left\{ \frac{x}{\beta}(h + y) \cos^{-1}\left[\frac{(1 - \beta m)}{(1 + \beta m)} + \frac{2\beta y}{x(\beta m + 1)} \right] + \left[h + y \frac{(3\beta m + 1)}{3(\beta m + 1)} - \right. \right.$$

$$\left. \left. \frac{2x}{3\beta(\beta m + 1)} \right] \sqrt{ \frac{2}{(1 + \beta m)} \left[\frac{x^2}{\beta^2} - y^2 + \frac{(\beta m - 1)}{(\beta m + 1)}\left(\frac{x}{\beta} + y\right)^2 \right] } \right\} \tag{6}$$

Performing the chordwise integration of $\partial\varphi/\partial x$ indicated in equation (4) gives $C_{l_{p_2}}$ and $C_{l_{p_3}}$ expressed as integrals of the span loads. The last integration (spanwise) was done numerically.

$$C_{l_{p_2}} = \frac{16}{\pi S b^2} \int_{-\frac{c_t}{\beta}}^{0} dy(y+h) \left\{ \frac{c_t}{\beta}(h+y)\cos^{-1}\left[\frac{2\beta y}{c_t(\beta m + 1)} + \frac{(1-\beta m)}{(1+\beta m)}\right] + \pi y(h+y) + \right.$$

$$\left. \left[h + y\frac{(3\beta m + 1)}{3(\beta m + 1)} - \frac{2c_t}{3\beta(\beta m + 1)}\right]\sqrt{\frac{2}{(1+\beta m)}\left[\frac{c_t^2}{\beta^2} - y^2 + \frac{(\beta m - 1)}{(\beta m + 1)}\left(\frac{c_t}{\beta} + y\right)^2\right]}\right\} \quad (7)$$

$$C_{l_{p_3}} = \frac{16}{\pi S b^2} \int_{0}^{mc_a} dy(y+h) \left\{ \frac{c_a}{\beta}(h+y)\cos^{-1}\left[\frac{2\beta y}{c_a(\beta m + 1)} + \frac{1-\beta m}{1+\beta m}\right] + \right.$$

$$\left. \left[h + y\frac{(3\beta m + 1)}{3(\beta m + 1)} - \frac{2c_a}{3\beta(\beta m + 1)}\right]\sqrt{\frac{2}{(1+\beta m)}\left[\frac{c_a^2}{\beta^2} - y^2 + \frac{(\beta m - 1)}{(\beta m + 1)}\left(\frac{c_a}{\beta} + y\right)^2\right]}\right\} \quad (8)$$

Therefore,

$$C_{l_{p_{Total}}} = C_{l_{p_1}} + C_{l_{p_2}} + C_{l_{p_3}} \quad (9)$$
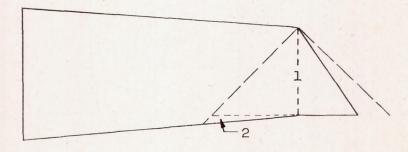
The potential $\varphi_{2,3}$ is not correct in the small shaded area of region 2; consequently an error, believed to be small as in the case of $C_{l_{\delta_2}}$, will be introduced. The error in $\frac{pb}{2V}\Big/\delta$ due to this procedure will be reduced since $\frac{pb}{2V}\Big/\delta$ is the result of the ratio $C_{l_\delta}\Big/C_{l_p}$. The combined effect in the case calculated is believed to increase $\frac{pb}{2V}\Big/\delta$ by about 5 percent to 10 percent.

In summation $\frac{pb}{2V}\Big/\delta$ may be expressed as

$$\frac{pb/2V}{\delta} = \frac{C_{l_{\delta_{Total}}}}{C_{l_{p_{Total}}}} = \frac{C_{l_{\delta_1}} + C_{l_{\delta_2}}}{C_{l_{p_1}} + C_{l_{p_2}} + C_{l_{p_3}}} \tag{10}$$

UNSWEPT TAPERED WING

The unswept-tapered-wing calculations were more involved than those for the rectangular wing and fewer of the expressions are given in closed form. The technique, however, is essentially the same.

Rolling-Moment Effectiveness Coefficient C_{l_δ}

The total C_{l_δ} for the wing in the preceding sketch was determined as before by combining the rolling-moment contributions of regions 1 and 2. The expression for $C_{l_{\delta_1}}$ obtained for the rectangular wing is applicable in this case also.

$$Cl_{\delta_1} = \frac{4\sqrt{\beta m}}{\beta} \frac{S_a}{Sb}\left[h + \frac{c_a}{6\beta}(3\beta m - 1)\right] \tag{11}$$
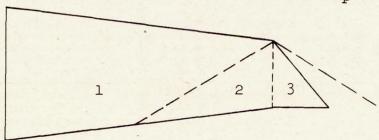
The coefficient Cl_{δ_2} is expressed as the integral of the chordwise load and must, therefore, be evaluated numerically.

$$Cl_{\delta_2} = \frac{16(\beta m)^{3/2}}{\beta^2 \pi Sb(\beta m + 1)} \int_{c_t}^{\frac{\beta c_t}{\beta-k}} dx \left\{ \frac{(\beta m + 1)}{2}\left[hx + \frac{(3\beta m - 1)x^2}{4\beta}\right] \cos^{-1}\left[\frac{-2\frac{\beta}{k}(c_t - x) + x(\beta m - 1)}{x(\beta m + 1)}\right] - \right.$$

$$\left[h + \frac{c_t}{2k} + \frac{x}{4\beta}\left(3\beta m + 1 - 2\frac{\beta}{k}\right)\right]\sqrt{x^2\left[\beta m - \frac{\beta}{k}(\beta m - 1) - \frac{\beta^2}{k^2}\right] + c_t x\left[\frac{\beta}{k}(\beta m - 1) + 2\frac{\beta^2}{k^2}\right] - \frac{\beta^2 c_t^2}{k^2}} \right\} \tag{12}$$

$$Cl_{\delta_{Total}} = Cl_{\delta_1} + Cl_{\delta_2} \tag{13}$$

Damping-in-Roll Coefficient Cl_p

The total Cl_p of the wing shown in the preceding sketch was obtained by combining the respective rolling-moment contributions of the areas denoted in the sketch. The

coefficient $C_{l_{p_1}}$ was not readily obtained in closed form; however, $C_{l_{p_A}}$ for a wing of the above plan form without the aileron may be obtained from reference 8. The pressure in the tip region of the above wing (without aileron) is given on page 7 of reference 9 as

$$C_p = \frac{8p}{\pi V \sqrt{\beta - k^2}} \left\{ \left[hx + \frac{\beta^2 xy}{\left(\beta^2 - k^2\right)} - \frac{kx^2}{2\left(\beta^2 - k^2\right)} \right] \cos^{-1}\sqrt{\frac{x + \beta y}{x - ky}} + \right.$$

$$\sqrt{-y(\beta + k)(x + \beta y)} \left[\frac{y\left(4\beta^2 + 2\beta k - 3k^2\right)}{3\left(\beta^2 - k^2\right)} - \frac{x(2\beta + k)}{3\left(\beta^2 - k^2\right)} + 2h \right] +$$

$$\left. \tan^{-1}\sqrt{\frac{x + \beta y}{-y(\beta + k)}} \left[\frac{ky^2\left(2\beta^2 - k^2\right)}{\left(\beta^2 - k^2\right)} + 2hyk \right] \right\}$$

The axis and symbol notation have been changed to conform with those of the present paper. After integrating this pressure in the chordwise direction $C_{l_{p_B}}$ may be expressed as the integral of the chordwise loads.

$$C_{l_{p_B}} = \frac{32}{\pi S b^2 \sqrt{\beta^2 - k^2}} \int_{\frac{c_t}{k-\beta}}^{0} dy(y + h) \left\{ ky\left[h + y\frac{\left(2\beta^2 - k^2\right)}{2\left(\beta^2 - k^2\right)}\right] \tan^{-1}\sqrt{\frac{c_t + y(\beta - k)}{-y(\beta + k)}} + \right.$$

$$\left(c_t - ky\right)\left[h + \frac{\left(2\beta^2 y + k^2 y - kc_t\right)}{2\left(\beta^2 - k^2\right)}\right] \cos^{-1}\sqrt{\frac{c_t + y(\beta - k)}{c_t - 2ky}} + \left[\beta yh + \frac{\beta^2 y^2(2\beta + k)}{2\left(\beta^2 - k^2\right)}\right]\frac{\pi}{2} +$$

$$\left. \left[h + y\frac{\left(2\beta^2 + 2\beta k - 3k^2\right)}{6\left(\beta^2 - k^2\right)} - \frac{\left(c_t - ky\right)(4\beta + k)}{6\left(\beta^2 - k^2\right)}\right]\sqrt{y(\beta + k)\left[c_t + y(\beta - k)\right]} \right\} \quad (14)$$

Therefore,

$$C_{l_{p_1}} = \frac{S_o}{S} \frac{2h^2}{b} \left(C_{l_{p_A}} - C_{l_{p_B}} \right)$$

(15)

The potential in regions 2 and 3 was obtained by Evvard's method (reference 7).

$$\varphi_{2,3} = \frac{p}{\pi} \left(\left[\frac{2h(x - ky)}{(\beta - k)} + \right. \right.$$

$$\left. \frac{-kx^2 + 2\beta^2 xy - ky^2(2\beta^2 - k^2)}{(\beta + k)(\beta - k)^2} \right] 2\sqrt{\frac{\beta - k}{\beta + k}} \cos^{-1} \left[\frac{(\beta + k)(1 - \beta m)\left(\frac{x}{\beta} + y\right) + (\beta m + 1)\left(\beta y - \frac{kx}{\beta}\right)}{(\beta m + 1)(x - ky)} \right] +$$

$$\left\{ h - \frac{\left(y + \frac{x}{\beta}\right)}{8} \left[\frac{\beta - k}{\beta + k} + \frac{4(1 - \beta m)(2\beta - k)}{2(\beta m + 1)(\beta - k)} \right] + \frac{\left(8y - \frac{x}{\beta}\right)}{12} + \right.$$

$$\left. \frac{(\beta + k)\left(y - \frac{x}{\beta}\right)}{8(\beta - k)} \right\} \sqrt{\frac{2\beta(1 - mk)}{(\beta - k)(\beta m + 1)} \left[\frac{x^2}{\beta^2} - y^2 + \frac{(\beta m - 1)}{(\beta m + 1)}\left(\frac{x}{\beta} + y\right)^2 \right]} \right)$$

(16)

Upon performing the chordwise integration of $\partial\varphi/\partial x$ indicated in equation (4), $C_{l_{p_2}}$ and $C_{l_{p_3}}$ may be expressed as the integrals of the spanwise loads. The integrations were carried out numerically.

$$Cl_{p_2} = \frac{16}{\pi Sb^2} \int_{\frac{c_t}{(k-\beta)}}^{0} (y+h)dy \left(\frac{1}{2\sqrt{k_1}} \left[2k_1 hy + \frac{k_1(3+k_1)y^2}{2} \right] \pi \frac{1}{2\sqrt{k_1}} \left\{ h \left[\left(\frac{c_t}{\beta} - \frac{ky}{\beta} \right)(1+k_1) + \right. \right. $$

$$\left. y(1-k_1) \right] + \frac{1}{8k_1} \left[\frac{(c_t - ky)^2(1+k_1)^2(1-k_1)}{\beta^2} + 2y\left(\frac{c_t}{\beta} - \frac{ky}{\beta} \right)(1+k_1)^3 + \right.$$

$$\left. y^2(1-k_1)(1+6k_1+k_1{}^2) \right] \right\} \cos^{-1} \left[\frac{\left(1 + \frac{2k_1}{k_2} - k_1 \right)\left(\frac{c_t}{\beta} - \frac{ky}{\beta} \right) + \left(1 + \frac{2k_1}{k_2} + k_1 \right)y}{(1+k_1)\left(\frac{c_t}{\beta} - \frac{ky}{\beta} \right) + (1-k_1)y} \right] + $$

$$\frac{1}{2\sqrt{k_1}} \left[h - \frac{\left(y + \frac{c_t}{\beta} - \frac{ky}{\beta} \right)}{8} \left(\frac{1}{k_1} + \frac{2}{k_2} + \frac{2k_1}{3k_2} \right) + \frac{\left(8y - \frac{c_t}{\beta} + \frac{ky}{\beta} \right)}{12} + \frac{k_1}{8}\left(y - \frac{c_t}{\beta} + \right. \right.$$

$$\left. \left. \frac{ky}{\beta} \right) \right] \sqrt{\left(1 + \frac{k_1}{k_2} \right) \left[\frac{(c_t-ky)^2}{\beta^2} - y^2 - \frac{(c-ky+y)^2}{\beta^2 k_2} \right]} \right) \tag{17}$$

where

$$k_1 = \frac{\beta+k}{\beta-k}$$

$$k_2 = \frac{1+\beta m}$$

$$C_{l_{p_3}} = \frac{16}{\pi S b^2} \int_0^{mc} (y + h)dy \left(\frac{1}{2\sqrt{k_1}} \left\{ h\left[\frac{c_t}{\beta}\left(1 + k_1\right) + y\left(1 - k_1\right)\right] + \frac{1}{8k_1}\left[\frac{c_t^2}{\beta^2}\left(1 + k_1\right)^2\left(1 - k_1\right) + \right.\right.\right.$$

$$\left.\left. \frac{2c_t y}{\beta}\left(1 + k_1\right)^3 + y^2\left(1 - k_1\right)\left(1 + 6k_1 + k_1^2\right)\right]\right\} \cos^{-1}\left[\frac{\left(1 + \frac{2k_1}{k_2} - k_1\right)\frac{c_t}{\beta} + \left(1 + \frac{2k_1}{k_2} + k_1\right)y}{\left(1 + k_1\right)\frac{c_t}{\beta} + \left(1 - k_1\right)y}\right] +$$

$$\left[h - \frac{\left(y + \frac{c_t}{\beta}\right)}{8}\left(\frac{1}{k_1} + \frac{2}{k_2} + \frac{2k_1}{3k_2}\right) + \frac{\left(8y - \frac{c_t}{\beta}\right)}{12} + \frac{k_1}{8}\left(y - \frac{c_t}{\beta}\right)\right] \sqrt{\left(1 + \frac{k_1}{k_2}\right)\left[\frac{c_t^2}{\beta^2} - y^2 - \frac{\left(\frac{c_t}{\beta} + y\right)^2}{k_2}\right]}\right)$$

(18)

Therefore,

$$C_{l_{p_{Total}}} = C_{l_{p_1}} + C_{l_{p_2}} + C_{l_{p_3}}$$

In summation

$$\frac{pb/2V}{\delta} = \frac{C_{l_{\delta_{Total}}}}{C_{l_{p_{Total}}}} = \frac{C_{l_{\delta_1}} + C_{l_{\delta_2}}}{C_{l_{p_1}} + C_{l_{p_2}} + C_{l_{p_3}}}$$

REFERENCES
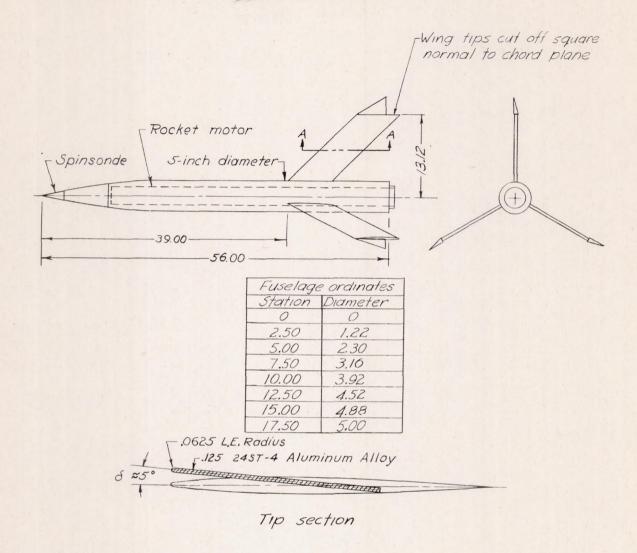
1. Sandahl, Carl A., and Strass, H. Kurt: Comparative Tests of the Rolling Effectiveness of Constant-Chord, Full-Delta, and Half-Delta Ailerons on Delta Wings at Transonic and Supersonic Speeds. NACA RM L9J26, 1949.

2. Sandahl, Carl A., and Marino, Alfred A.: Free-Flight Investigation of Control Effectiveness of Full-Span 0.2-Chord Plain Ailerons at High Subsonic, Transonic, and Supersonic Speeds to Determine Some Effects of Section Thickness and Wing Sweepback. NACA RM L7D02, 1947.

3. Harris, Orville R.: Determination of the Rate of Roll of Pilotless Aircraft Research Models by Means of Polarized Radio Waves. NACA TN 2023, 1950.

4. Strass, H. Kurt: The Effect of Spanwise Aileron Location on the Rolling Effectiveness of Wings with 0° and 45° Sweep at Subsonic, Transonic, and Supersonic Speeds. NACA RM L50A27, 1950.

5. Lagerstrom, P. A., and Graham, Martha E.: Linearized Theory of Supersonic Control Surfaces. Jour. Aero. Sci., vol. 16, no. 1, Jan. 1949, pp. 31-34.

6. Harmon, Sidney M.: Stability Derivatives at Supersonic Speeds of Thin Rectangular Wings with Diagonals ahead of Tip Mach Lines. NACA Rep. 925, 1949.

7. Evvard, John C.: Distribution of Wave Drag and Lift in the Vicinity of Wing Tips at Supersonic Speeds. NACA TN 1382, 1947.

8. Piland, Robert O.: Summary of Theoretical Lift, Damping-in-Roll, and Center-of-Pressure Characteristics of Various Wing Plan Forms at Supersonic Speeds. NACA TN 1977, 1949.

9. Tucker, Warren A., and Nelson, Robert L.: The Effect of Torsional Flexibility on the Rolling Characteristics at Supersonic Speeds of Tapered Unswept Wings. NACA Rep. 972, 1950.

CONFIDENTIAL

TABLE I

SUMMARY OF CONFIGURATIONS TESTED

Configuration	A	$\Lambda_{c/2}$ (deg)	λ_w	i (deg)	δ (deg)
1	5.28	0	1.0	0.01	4.9
2	5.28	45	1.0	0.04	4.8
3	4.94	0	.45	-0.12	5.0
4	4.94	45	.45	-0.01	4.3
5	4.94	0	.45	-0.05	5.0

NACA

Wing tips cut off square
normal to chord plane

Rocket motor

Spinsonde   5-inch diameter

A   A

13.12

39.00

56.00

Fuselage ordinates	
Station	Diameter
0	0
2.50	1.22
5.00	2.30
7.50	3.16
10.00	3.92
12.50	4.52
15.00	4.88
17.50	5.00

.0625 L.E. Radius

.125 24ST-4 Aluminum Alloy

$\delta \approx 5°$

Tip section

.020 steel inlay covered
with 1/32 veneer

.125 Aluminum Alloy

2

.1c   .2c

Typical Section A-A   NACA

NACA 65A009
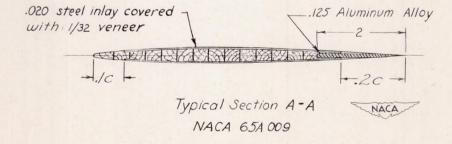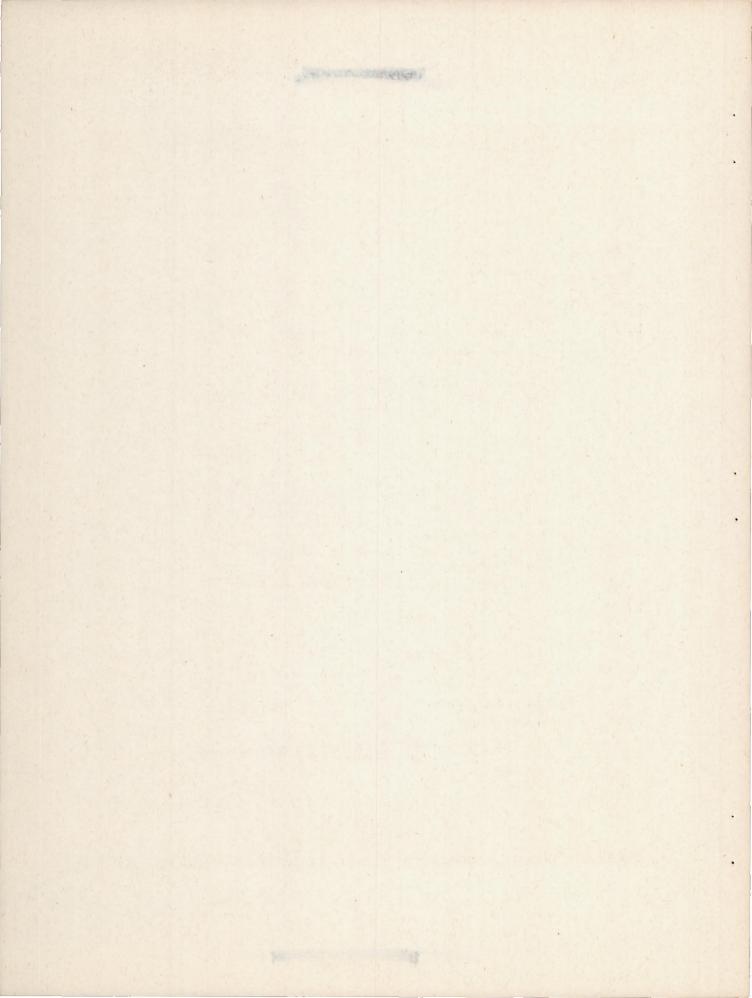
Figure 1.- General arrangement of test vehicles.   All dimensions are in
inches.
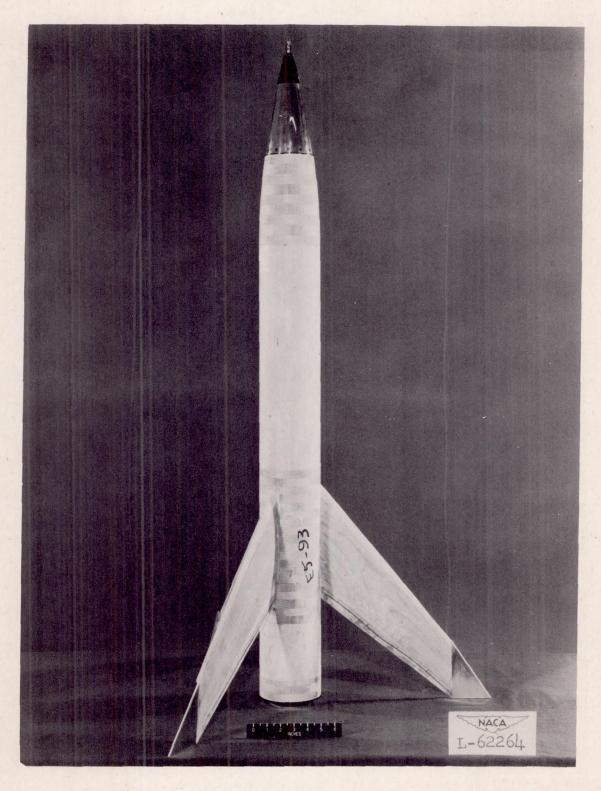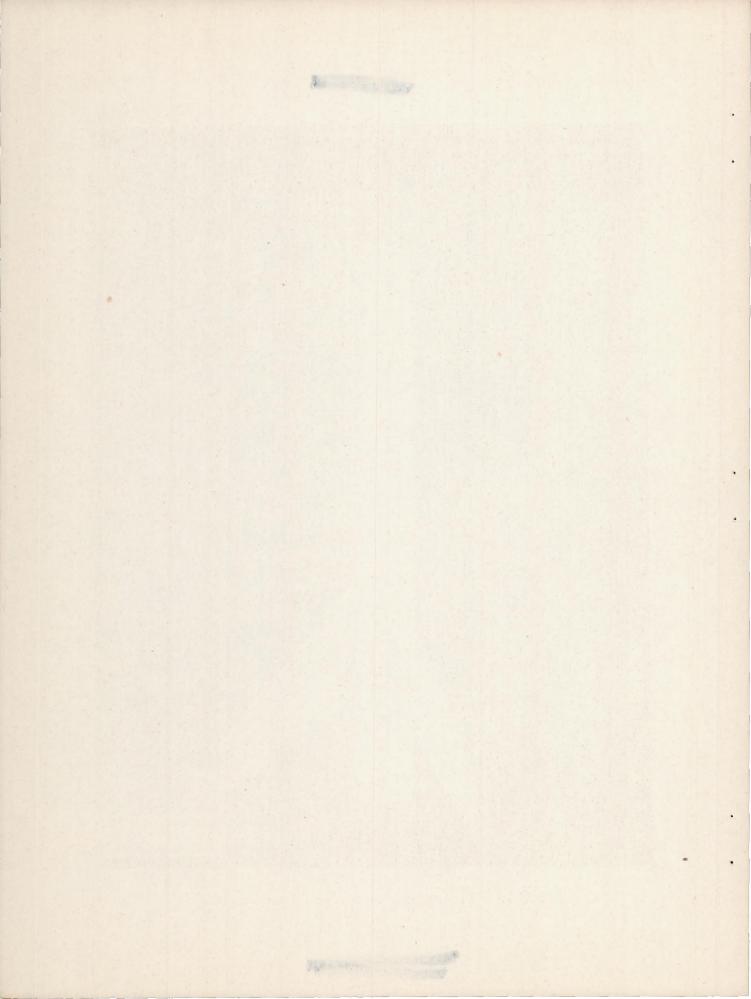
Figure 2.- Photograph of typical test vehicle.
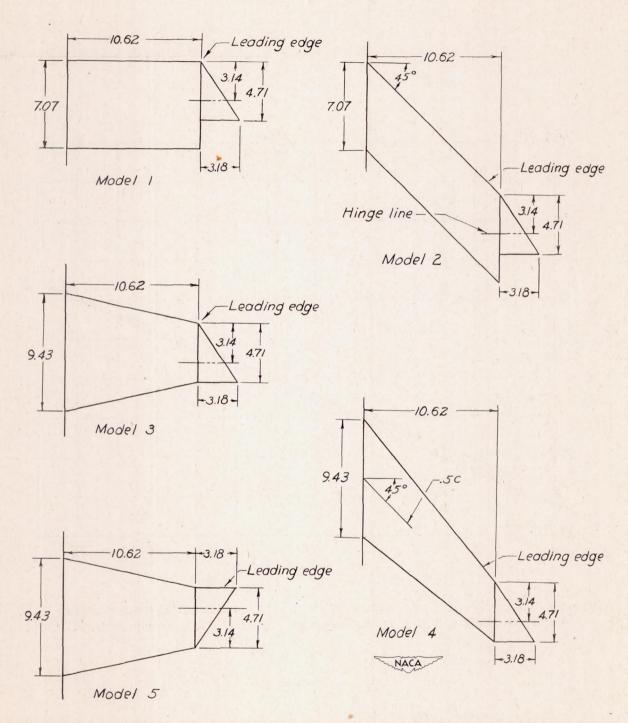
Figure 3.- Sketches of wing configurations. All dimensions are in inches.
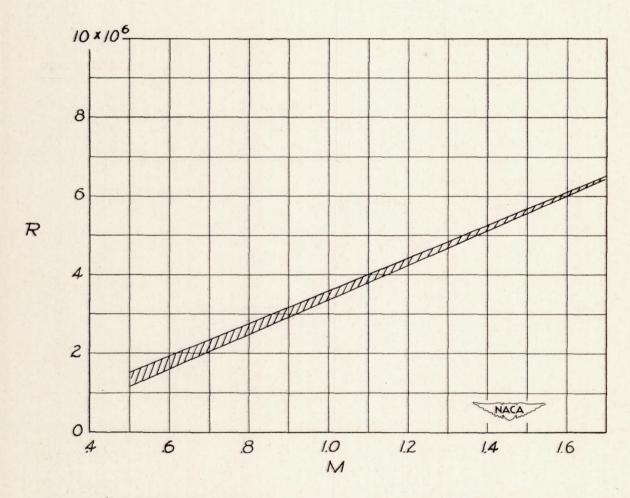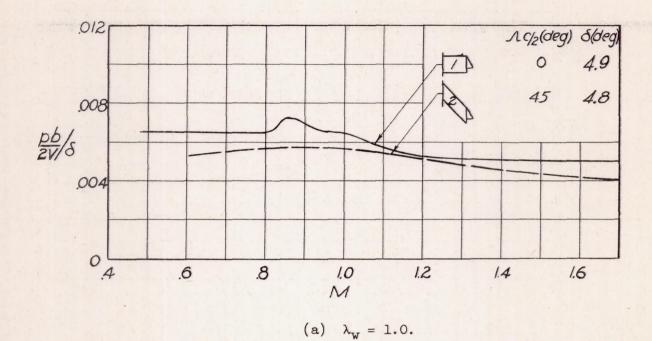
Figure 4.- Range and variation of Reynolds number with Mach number.
Reynolds number based on an average exposed wing chord of 0.58 foot.

(a) $\lambda_w = 1.0$.

(b) $\lambda_w = 0.45$.
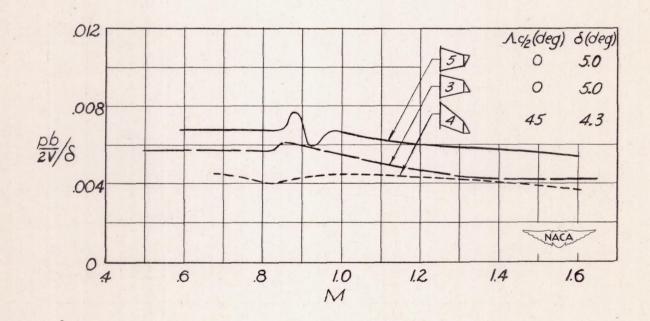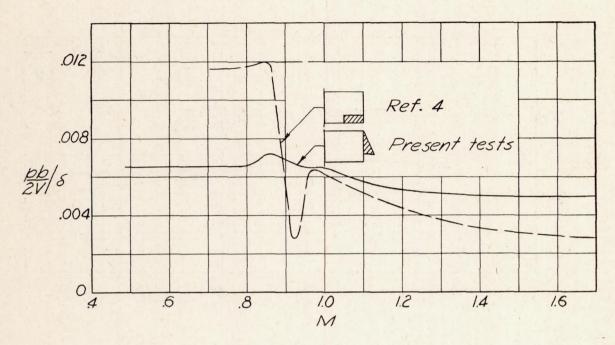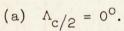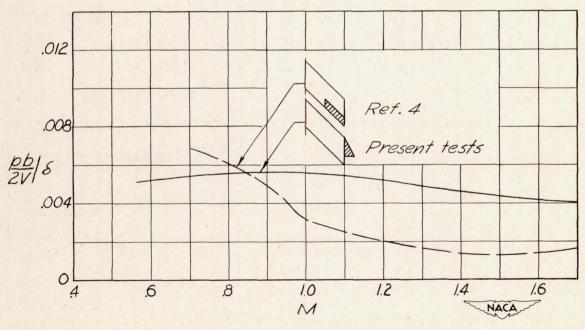
Figure 5.- Variation of rolling effectiveness with Mach number.

(a) $\Lambda_{c/2} = 0^{\circ}$.
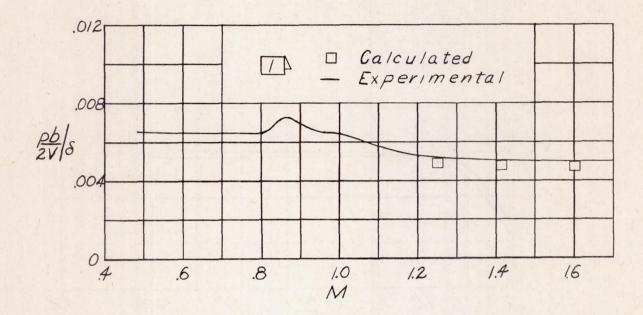
(b) $\Lambda_{c/2} = 45^{\circ}$.

Figure 6.- Comparison of rolling effectiveness of plain and half-delta tip ailerons.
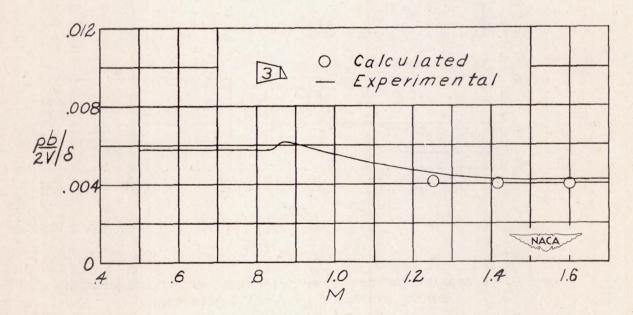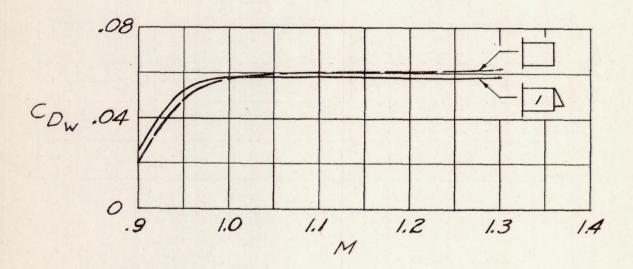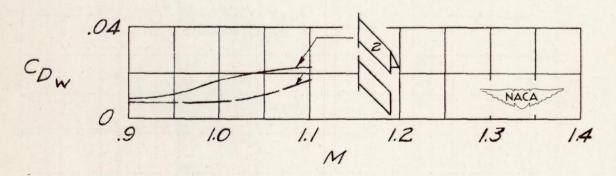
Figure 7.- Comparison of experimental results with theoretical calculations.
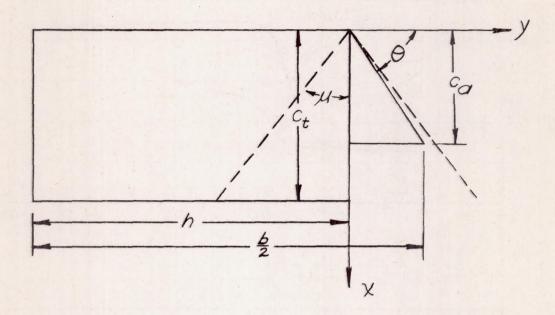
(a) $\Lambda_{c/2} = 0^{\circ}$.

(b) $\Lambda_{c/2} = 45^{\circ}$.

Figure 9.- Comparison of drag coefficients of wing configurations
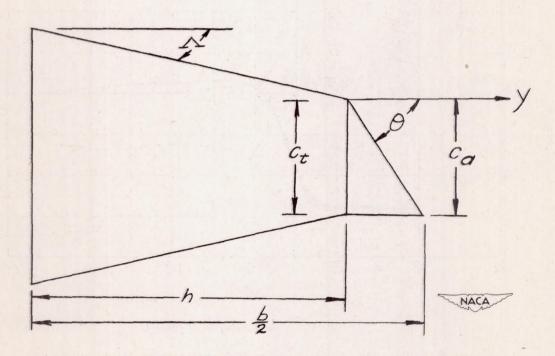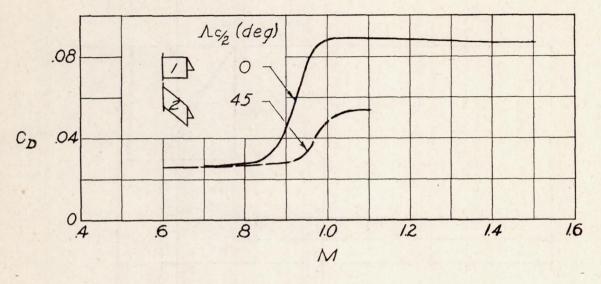having plain and half-delta ailerons.

Figure 10.- The configurations investigated theoretically.
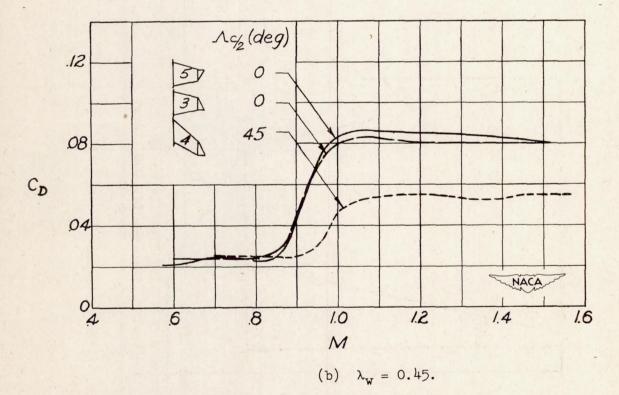
(a) $\lambda_W = 1.0$.

(b) $\lambda_W = 0.45$.

Figure 8.- Variation of drag coefficient with Mach number.